

Supplementary information

Plasmon Enhanced Upconverting Core@Triple-Shell Nanoparticles as Recyclable Panchromatic Initiator (Blue to Infrared) for Radical Polymerization

Jianming Zhang,[†] Yue Huang,[†] Xin Jin,[†] Artem Nazartchouk, Maosong Liu, Xin Tong, Yinhua Jiang, Liang Ni, Shuhui Sun, Yuanhua Sang, Hong Liu Luca Razzari* Fiorenzo Vetrone* and Jerome Claverie**

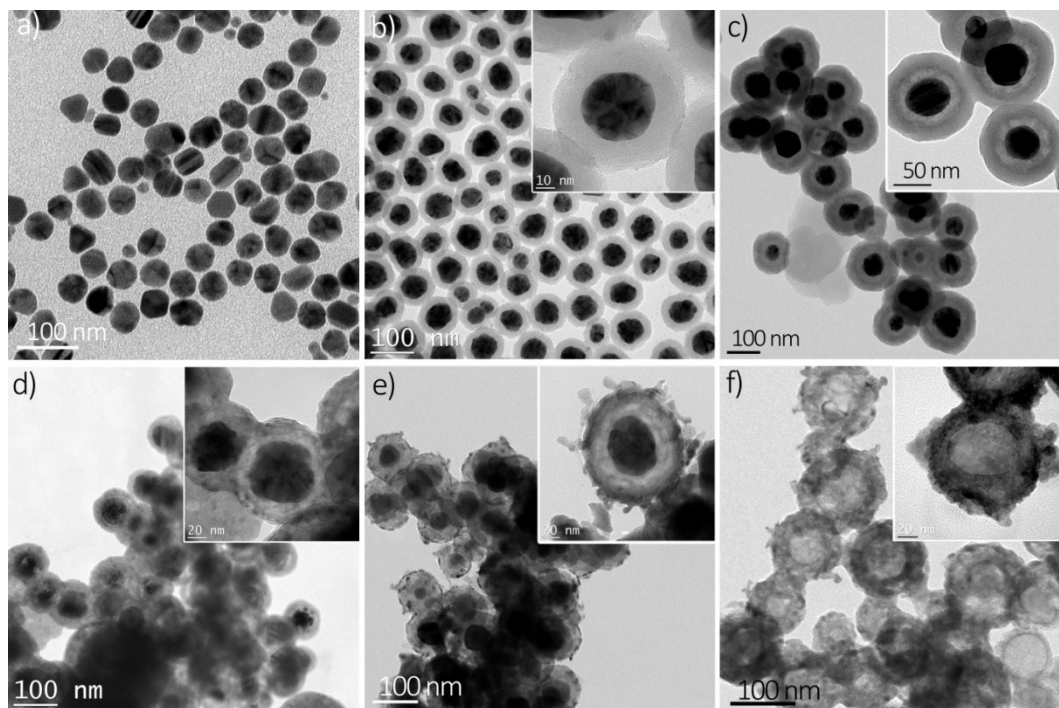


Figure S1. TEM images of (a) Ag, (b) Ag@SiO₂, (c) Ag@SiO₂@Y,Yb,Er(OH)CO₃, (d) Ag@SiO₂@UC, (e) Ag@SiO₂@UC@BFO and (f) SiO₂@UC@BFO nanostructures.

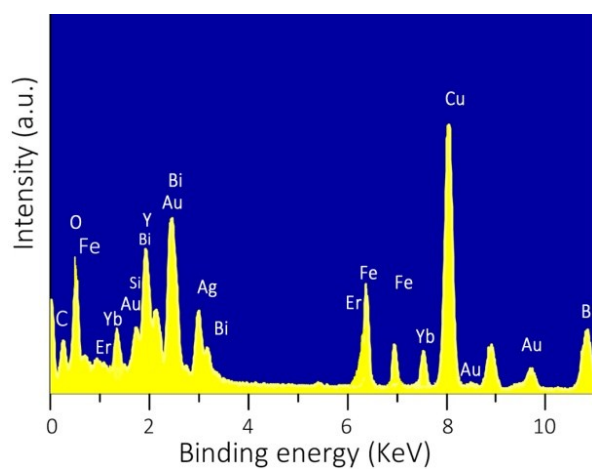


Figure S2. EDX spectrum of the Ag@SiO₂@UC@BFO-Au nanohybrids.

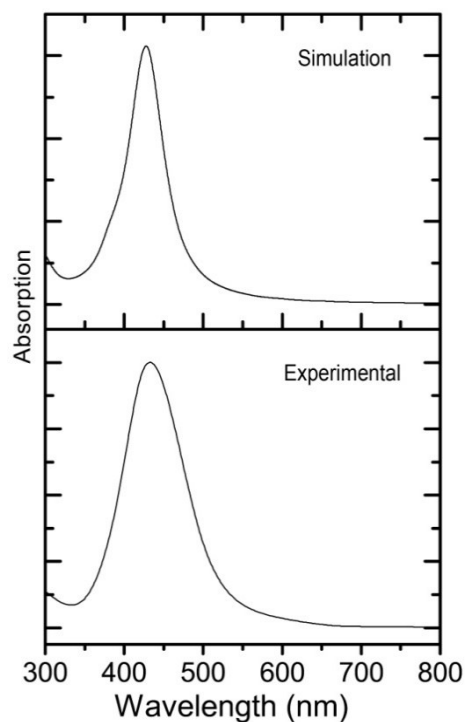


Figure S3. UV-VIS absorption spectra of 50 nm Ag NPs obtained from simulations (upper) and experimental data (lower graph).

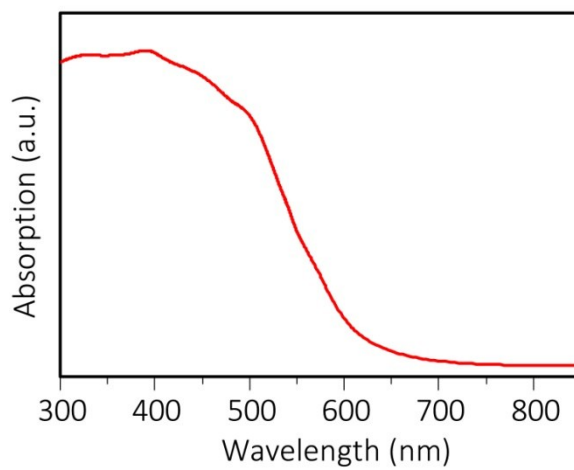


Figure S4. UV-VIS absorption spectrum of BFO.

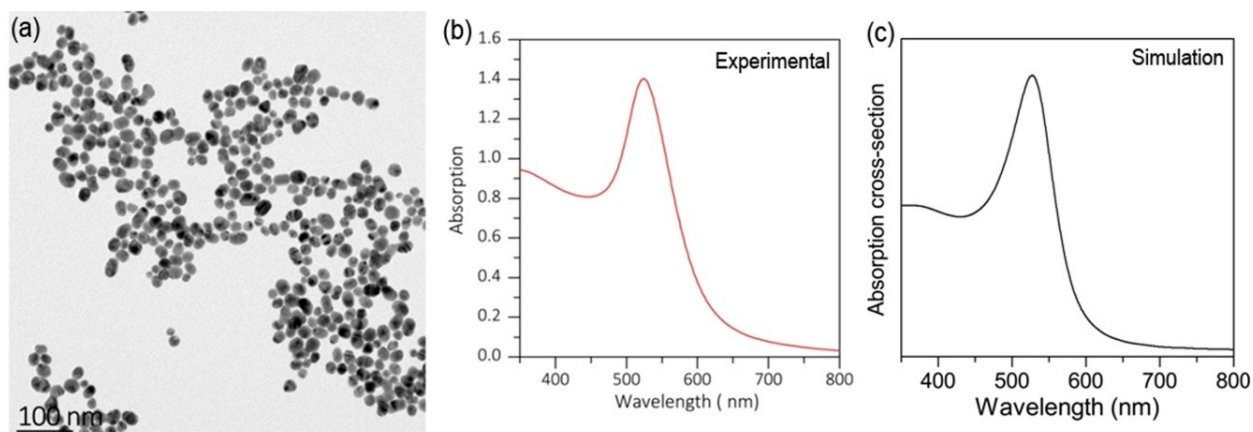


Figure S5. TEM image (a) of Au NPs and their UV-VIS absorption spectrum obtained experimentally (b) and by simulation (unit m^{-2}) (c). The average diameter of the Au NPs is ~ 20 nm. The SPR peak position of the Au NPs is located at ~ 524 nm.

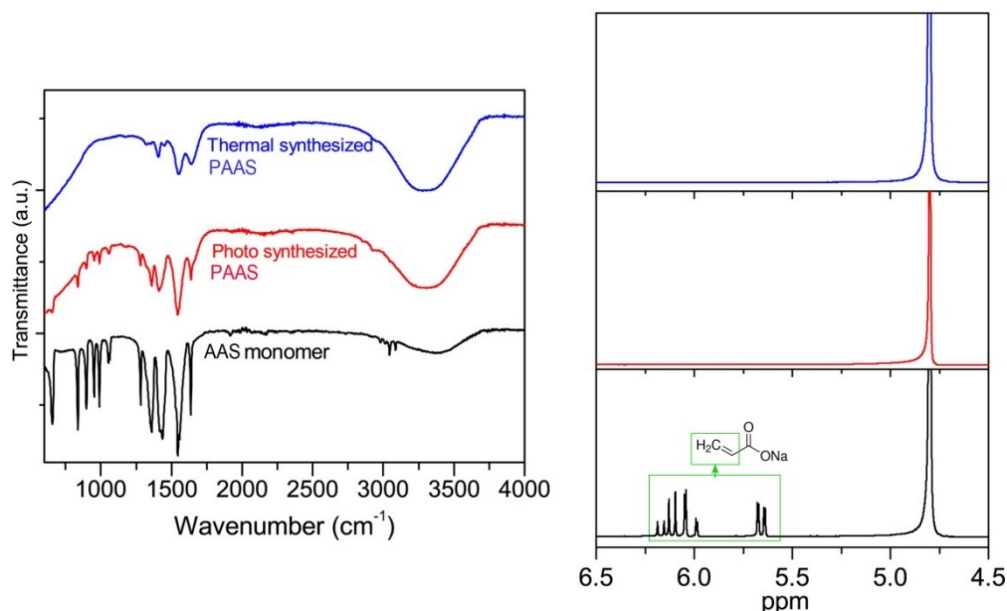


Figure S6. FTIR (left) and ^1H -NMR (right) spectra of AAS monomer, photo and thermal synthesized PAAS. The complex peaks at $500\text{-}1700\text{ cm}^{-1}$ assigned to AAS monomer became unnoticeable after the reaction, indicating a polymerization. The NMR spectrum of SA shows typical resonance signals of terminal vinyl protons ($\text{CH}_2=\text{CH}-$) of acryloyl groups (chemical shift at $\sim 5.70 - 6.30$ ppm). After polymerization, the signals of vinyl protons disappeared, indicating a successful polymerization.

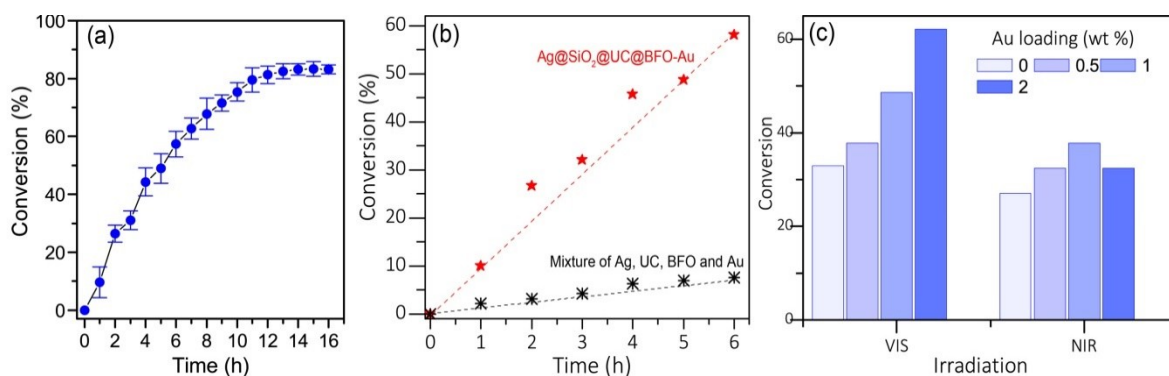


Figure S7. (a) Photo-polymerization conversion ratio as a function of irradiation time. (b) Photo-polymerization of AAS under VIS light using Ag@SiO₂@UC@BFO-Au and the mixture of Ag, UC, BFO and Au as the initiator. (c) Au loading effect on the efficiency of photo-polymerization under VIS (6 h) and NIR (12 h) irradiation.

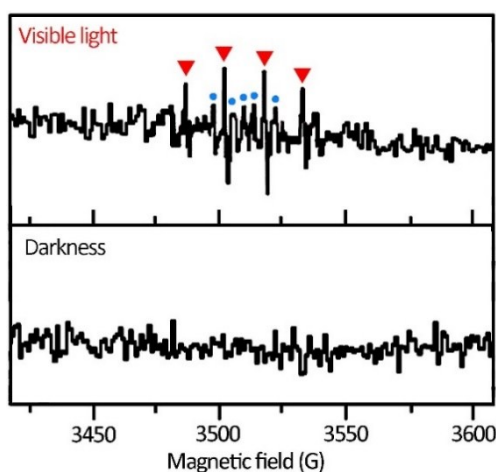


Figure S8. ESR spectrum of the Ag@SiO₂@UC@BFO-Au nanohybrids with DMPO in darkness (lower) and VIS light irradiation for 10 min (upper). Red triangle marks the signal for OH• radicals.

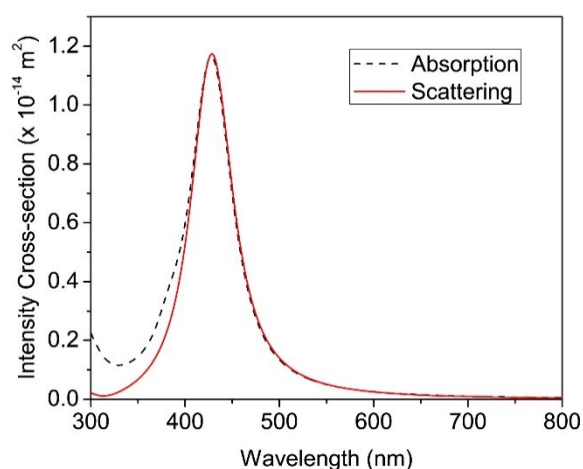


Figure S9. Simulation results of absorption and scattering spectra of the 50 nm Ag NPs, where the strong light scattering of the NP (comparable to the absorption) is evidenced.

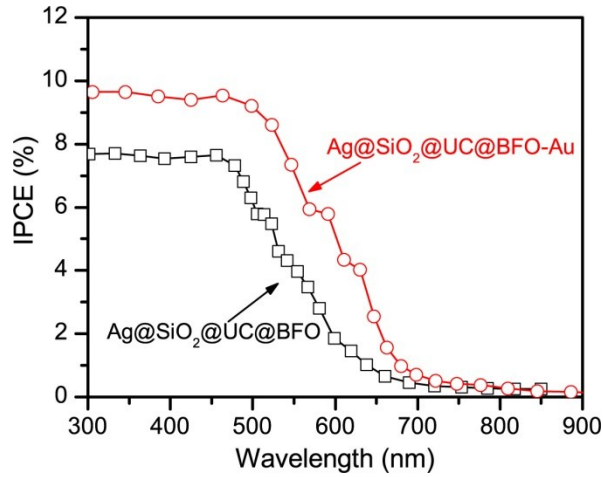


Figure S10. IPCE spectra of Ag@SiO₂@UC@BFO before (black) and after Au decoration (red).

Table S1. The key elemental content of the Ag@SiO₂@UC@BFO-Au sample was analyzed using ICP-OES technique to 1 mg of sample. The measurement was repeated for 3 times, the mean values and standard deviation are listed (unit: mg). These results indicate that the quantity of the key components in the hybrid matches well with those in their precursor during synthesis.

Element	Au	Fe	Bi	Ag	Y
Content Determination	0.045 ± 0.020	0.032 ± 0.007	0.096 ± 0.010	0.152 ± 0.017	0.469 ± 0.090

2. Simulation Details

Electromagnetic simulations in this study were conducted by using the Finite Element Method based software – COMSOL Multiphysics, optics module [1]. As shown in Figure S11, the starting geometry was composed of a silver nanoparticle with the size of 50-nm enclosed in a 20-nm thick silica shell, then further covered by a Y₂O₃ layer of 10 nm and a subsequent 10-nm layer of BiFeO₃ (BFO). On the BFO surface, twelve gold nanoparticles (20-nm diameter) were evenly distributed following a regular icosahedron distribution, with each sphere having a single contact point to the surface of the BFO shell. This stratified structure was then submerged in a cube of water with perfectly matched layers covering all external boundaries to truncate the calculation domain while avoiding spurious reflections. For the illumination condition, a plane wave was sent from the positive direction of z-axis (see the coordinates in Figure S11) with polarization set along the x-axis. Thus, by considering the incident wave polarization and the y-z plane symmetry, we cut the entire model in half to reduce the total

computation time, in which a perfect electric conductor boundary condition was applied on the y-z plane for mirroring the model. In addition, for simulations of nanohybrids without gold nanoparticles, the model also had an x-z plane symmetry. Therefore, we could use a perfect magnetic conductor boundary condition to further reduce the model as a quarter of the original. The optical properties used for this simulation were taken from the following references: Ag [2], Au [2], BFO [3], H₂O [4], SiO₂ [5] and Y₂O₃ [6]. Notice that for the Y₂O₃ layer, Er/Yb doping was not considered in the electromagnetic simulations.

In the simulations, it is possible to investigate and extract separately light absorption in the different elements composing the hybrid structure. The absorption contributions of different parts of the nanohybrid are shown in Figure S12-a. For a comparison purpose, we also simulated the exact same structure but replaced the Ag core with the background water, and the corresponding absorption results are shown in Figure S12-b. The overall absorption of the other elements is slightly increased by the presence of the Ag core.

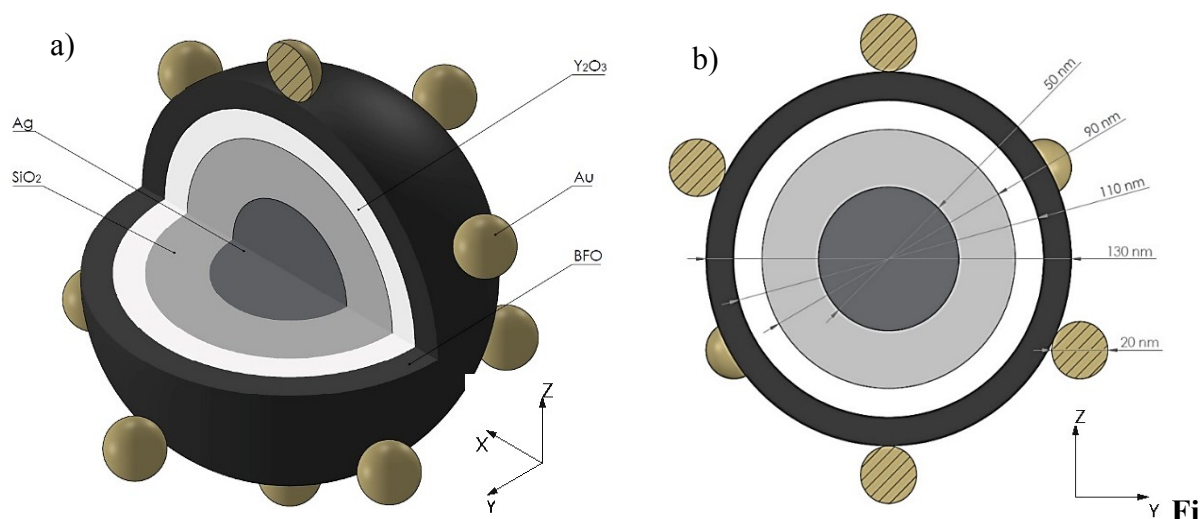


Figure S11. (a,b) Three-dimensional sketch of the simulated structure. Particles/shells sizes are shown in the y-z plane cross section.

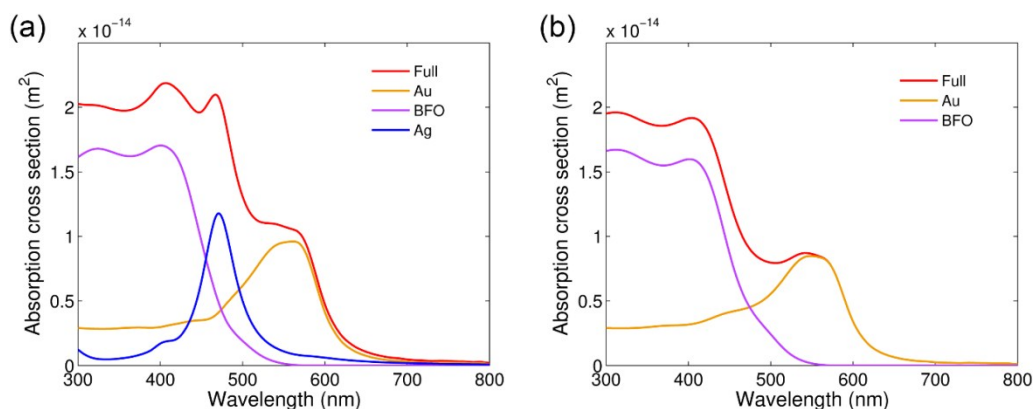


Figure S12. (a) Absorption cross sections for different elements in the same nanohybrid. (b) The same investigation for a structure in which the Ag core has been substituted with water.

References

- [1] “COMSOL Multiphysics® Modeling Software.” <https://www.comsol.com/>.
- [2] A. D. Rakić, A. B. Djurišić, J. M. Elazar, and M. L. Majewski, “Optical properties of metallic films for vertical-cavity optoelectronic devices,” *Appl. Opt.*, vol. 37, no. 22, pp. 5271–5283, Aug. 1998.
- [3] A. Kumar, R. C. Rai, N. J. Podraza, S. Denev, M. Ramirez, Y.-H. Chu, L. W. Martin, J. Ihlefeld, T. Heeg, J. Schubert, D. G. Schlom, J. Orenstein, R. Ramesh, R. W. Collins, J. L. Musfeldt, and V. Gopalan, “Linear and nonlinear optical properties of BiFeO₃,” *Appl. Phys. Lett.*, vol. 92, no. 12, p. 121915, Mar. 2008.
- [4] G. M. Hale and M. R. Querry, “Optical Constants of Water in the 200-nm to 200- μ m Wavelength Region,” *Appl. Opt.*, vol. 12, no. 3, pp. 555–563, Mar. 1973.
- [5] L. Gao, F. Lemarchand, and M. Lequime, “Refractive index determination of SiO₂ layer in the UV/Vis/NIR range: spectrophotometric reverse engineering on single and bi-layer designs,” *J. Eur. Opt. Soc. - Rapid Publ.*, vol. 8, no. 0, Jan. 2013.
- [6] Y. Nigara, “Measurement of the Optical Constants of Yttrium Oxide,” *Jpn. J. Appl. Phys.*, vol. 7, no. 4, p. 404, Apr. 1968.